

# Extrusion process of 304L H-shaped stainless steel used in passive residual heat removal heat exchanger

Lei-Feng Tuo<sup>1,2</sup> · Gen-Shu Zhou<sup>1</sup> · Zhi-Qiang Yu<sup>1</sup> · Xi-Tang Kang<sup>2</sup> · Bo-Wen Wang<sup>2</sup>

Received: 11 July 2018 / Revised: 2 October 2018 / Accepted: 20 October 2018 / Published online: 13 March 2019

© China Science Publishing & Media Ltd. (Science Press), Shanghai Institute of Applied Physics, the Chinese Academy of Sciences, Chinese Nuclear Society and Springer Nature Singapore Pte Ltd. 2019

**Abstract** 304L H-shaped stainless steel is used as the support frame of the passive residual heat removal heat exchanger (PRHR HX) in a nuclear fission reactor. The extrusion process is adopted to manufacture the 304L H-shaped stainless steel. Finite element method simulation is herein used to analyze metal flow characteristics, optimize the extrusion die, and predict the extrusion force at different temperatures and speeds. A  $\Phi 400$ -mm container and  $\Phi 388$ -mm forging billet are selected, and the 304L H-shaped stainless steel is successfully manufactured using a Germany SMS 60 MN horizontal extruder. The mechanical properties and microstructure of the manufactured 304L H-shaped stainless steel meet the requirements of the PRHR HX, and the surfaces of the product pass the dye penetration test. The H-shaped stainless steels are used in Haiyang nuclear power plant in Shandong Province.

**Keywords** PRHR HX · Support frame · Extrusion process · 304L · H-shaped stainless steel

## 1 Introduction

The passive safe system, which improves the safety and reliability of nuclear power plants, is generally used in third-generation nuclear technology. Current third-generation nuclear technology includes American AP1000 [1], European EPR [2], Chinese HPR1000 [3], etc. The passive residual heat removal heat exchanger [4] (PRHR HX) is a crucial piece of equipment that allows for passive cooling. When a power plant stops working in the event of a sudden accident such as a natural disaster, the PRHR HX rapidly discharges the residual heat to the external environment, which is important for the entire system as well as for the safety of the staff. Figure 1 shows the structures of the PRHR HX and its support frame.

Many stainless steels are used in the safety systems of nuclear power plants. Austenitic stainless steels are used in lead–bismuth eutectic (LBE) loops for integrated tests of operability and safety of proliferation-resistant, environment-friendly, accident-tolerant, continual, and economical reactors [5]. AISI 316L stainless steel pipes are used in lead–bismuth eutectic (LBE) loops for integrated tests of operability and safety [6]. 316LN is used as AP1000 primary coolant pipes [7]. H-shaped stainless steels are used in nuclear fission reactors as the support frames of residual heat removal exchangers, as shown in Fig. 2.

H-shaped stainless steels used in PRHR HX are generally manufactured by a welding process. Cai [8, 9] studied the manufacture of H-shaped stainless steel used as the support for AP1000 passive residual heat removal heat exchangers. The H-shaped stainless steel is first welded using three plates and then machined to its final size. Severe welding distortion occurs because residual stress

---

This work was supported by the State Key Laboratory for Mechanical Behavior of Materials (No. 20171909).

---

✉ Gen-Shu Zhou  
zhougenshuxjtu@163.com

<sup>1</sup> State Key Laboratory for Mechanical Behavior of Materials, Xi'an Jiaotong University, Xi'an 710049, China

<sup>2</sup> Stainless Steel Tube Branch Company, Taiyuan Iron & Steel (Group) CO. LTD, Taiyuan 030003, China

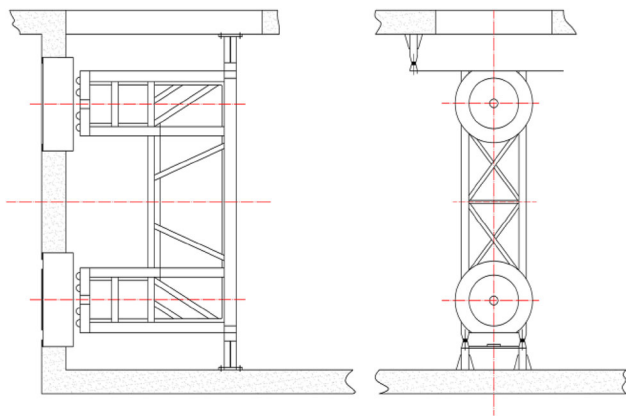


**Fig. 1** Passive residual heat removal heat exchanger

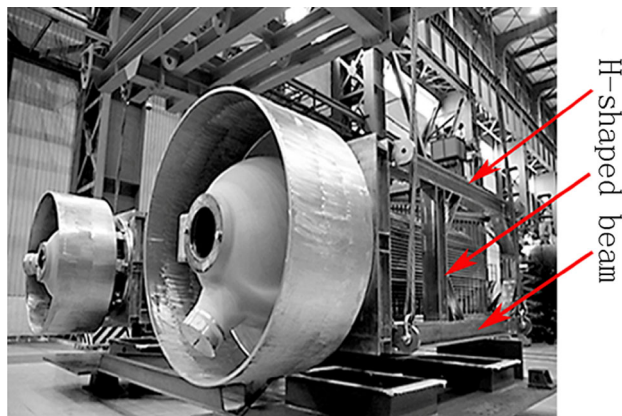


**Fig. 2** H-shaped stainless steel in a passive residual heat removal heat exchanger

exists in the H-shaped stainless steel after the welding process. Moreover, the plate cutting utilization efficiency and manufacturing efficiency are low. Wang [10, 11] studied the manufacturing process of the support frame of the PRHR HX. TP304 H-shaped stainless steel is also manufactured by a welding process, and it is very difficult to control the welding distortion. Besides, the welds in H-shaped stainless steel increase the risk to the PRHR HX, so it is necessary to develop another direct forming process (seamless H-shaped stainless steel) to replace the welding process.

In contrast to the welding process, the extrusion process avoids the welds, the performance of the product obtained is consistent, and the cost of the process is low. Moreover, three-dimensional compressive stress exists in the extrusion deformation process, the structure is homogeneous, the dimensions of the H-shaped stainless steel are accurate, and the surfaces of the H-shaped stainless steel are good because of glass lubrication.

In order to meet the requirements of the support frame of the residual heat removal exchanger in the Haiyang

nuclear power plant in Shandong province, China, the extrusion process of seamless 304L H-shaped stainless steel is herein studied.

## 2 Materials and methods

### 2.1 Material

The billet material is 304L stainless steel, which is manufactured using an ingot casting, radial forging, and machining process. Table 1 shows the key elemental constituents; the main alloy elements are Cr and Ni.

### 2.2 Extrusion model

304L H-shaped stainless steel is manufactured using an SMS 60 MN horizontal extruder. The extrusion model consists of an extrusion stem, container, block, billet, glass pad, and mold system, as shown in Fig. 3a. The mold system includes a die, cushion, and bolster, as shown in Fig. 3b. The cushion is also designed with an H-shaped hole, which is a key component to withstand the large extrusion force. Figure 3c shows a flat-die and a cone-die. The material of the die, cushion, and bolster is 4Cr5Mo-SiV1 (GB/T1299-2000).

### 2.3 Deformation design

The internal diameter of the extrusion container ' $D$ ' is  $\Phi 400$  mm. The thermal expansion coefficient ' $\mu$ ' is about 1.02–1.03 when austenite stainless steel is heated to 1373–1573 K. The thickness of the glass powder layer ' $h$ ' at the external surface of the 304L stainless steel billet is typically 0.5–1 mm. The diameter of the billet is smaller than the internal diameter of the container; the final diameter of the billet ' $D_1$ ' is  $\Phi 388$  mm [Eq. (1)]. The final sectional dimensions of the 304L H-shaped stainless steel are  $H211.5 \text{ mm} \times 229 \text{ mm} \times 15.5 \text{ mm} \times 25 \text{ mm}$ . The extrusion ratio ' $\lambda$ ' of the 304L H-shaped stainless steel is 9.4 [Eq. (2)]. ' $S_C$ ' is the sectional area of the internal diameter of the container, ' $S_H$ ' is the sectional area of the H-shaped stainless steel. Figure 4a, b shows the design drawings of the billet and the H-shaped stainless steel.

$$D = (D_1 - 2h)/\mu \quad (1)$$

$$\lambda = S_C/S_H \quad (2)$$

### 2.4 Heating process

In order to uniformly heat the 304L stainless steel billet uniformly, a circular furnace (Capital Engineering &

**Table 1** Key elemental constituents of 304L stainless steel

Element	C	Si	Mn	P	S	Cr	Ni	N	Co
%	0.03	0.27	2	0.018	0.001	18.22	8.15	0.06	0.02

**Fig. 3** (Color online) **a** Extrusion model, **b** mold system, and **c** flat-die and cone-die

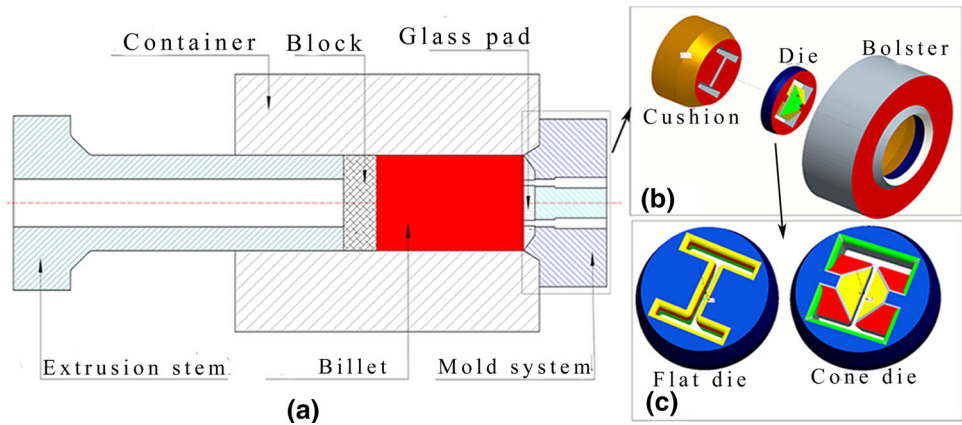


**Fig. 4** **a** Billet dimensions and **b** H-shaped stainless steel dimensions

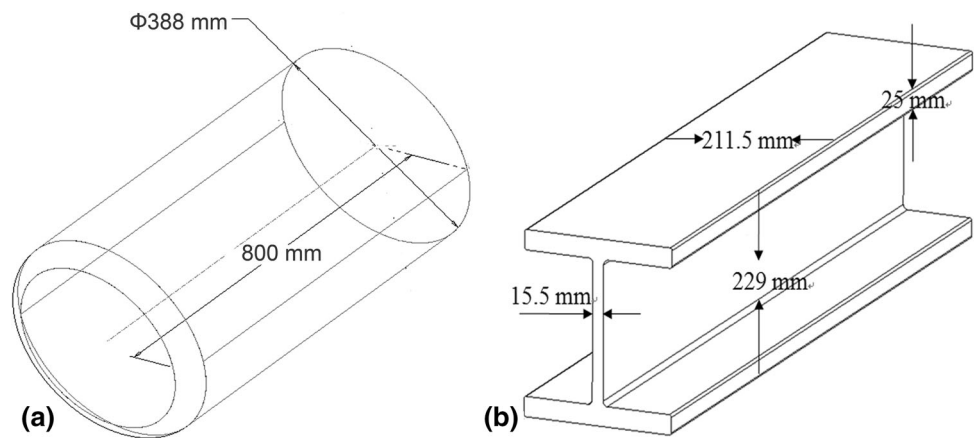
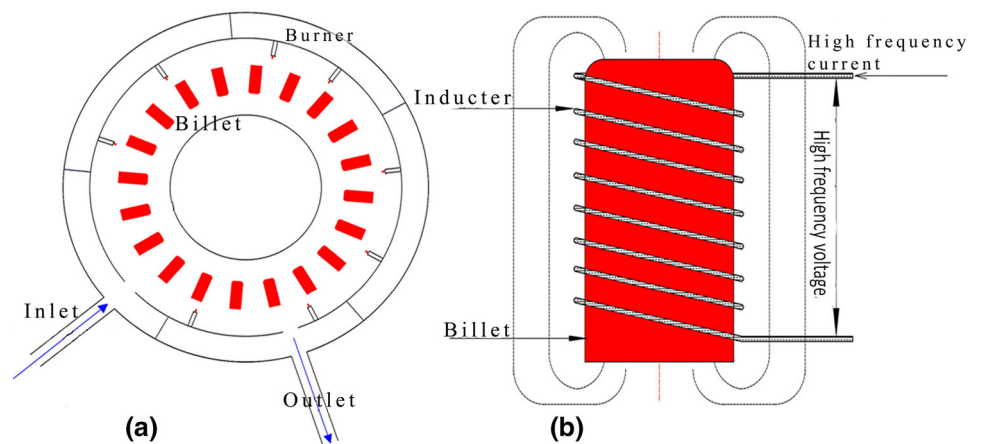


**Fig. 5** (Color online) **a** Circular furnace and **b** industrial frequency induction furnace



Research Incorporation Limited, China) (Fig. 5a) and an industrial frequency induction furnace (Inductotherm Banyard, USA) Fig. 5b are adopted.

### 2.5 Lubricant and lubrication method

In the hot extrusion process of stainless steel, glass lubrication serves to provide thermal insulation as well as

to reduce friction. Hansson [12] analyzed a finite element model of glass-lubricated extrusion of stainless steel tubes. Glass powder and glass pads are typically used as lubricants for stainless steel. Glass powder is used to lubricate the interface between the billet and the container; the billet will roll at the glass powder lubrication platform before extrusion begins. A glass pad is used to lubricate the extrusion die. Before flowing out the die hole, the metal must break the glass pad. The glass pad retards the deformation time significantly, in order to reduce the impact of the glass pad, an H-shaped glass pad is fabricated.

## 2.6 Simulation boundary conditions

In order to research the extrusion deformation process and predict the extrusion force of 304L H-shaped stainless steel, FEM simulation is used. The simulation process includes the definition of the materials, establishment of the model, and definition of the boundary conditions. 304L stainless steel in the material library of DEFORM-3D is used to define the billet material. Moreover, 4Cr5MoSiV1 is used to define the extrusion die, extrusion container, and ram.

Because glass powder and a glass pad are used as lubricants, the friction coefficient is set manually. Liu [13] studied the lubrication behavior of the glass-lubricated hot extrusion process and found the friction coefficient to be 0.03. The extrusion speed of the ram is defined between 150 mm/s and 400 mm/s, the extrusion temperature is defined between 1453 K and 1493 K, the finite mesh element is tetrahedral in shape, the solution step is defined with a time increment of 0.5 s, the primary die is ram, the solver is a conjugate-gradient, and the iteration method is direct iteration.

## 3 Results and discussion

### 3.1 Simulation results

#### 3.1.1 Metal flow characteristics

The metal flow characteristics of the flat-die and cone-die are different, as shown in Fig. 6. The metal flow of the flat-die is directed from the circle edge to the H-shaped die hole, but the metal flow of the cone-die obviously shunts from zone 'A' to zones 'B' and 'C'. In zones 'B' and 'C', the directions of metal flow are 'Y' and 'X', which are perpendicular to the edges of the H-shaped die hole.

The transitive characteristics of the forces on the flat-die and cone-die are different. In the flat-die, the directions of forces ' $F_A$ ', ' $F_B$ ', and ' $F_C$ ' are perpendicular to the upper surface of the flat-die, as shown in Fig. 7a. In the cone-die,

parts of the forces ' $F_A$ ' and ' $F_C$ ' are decomposed into ' $F_1$ ' and ' $F_2$ ', while the other parts of the forces ' $F_A$ ' and ' $F_C$ ' are perpendicular to the upper surface of the flat-die. ' $F_B$ ' is decomposed into ' $F_1$ ' and ' $F_2$ ', as shown in Fig. 7b. The decomposition of force reduces the extrusion force and effectively improves the service life of the die.

Five points, namely, 'P1', 'P2', 'P3', 'P4', and 'P5', are selected to track stress, strain, strain rate and velocity distribution during the extrusion process. 'P1', 'P2', and 'P3' are located in the formed H-shape stainless steel, and 'P4' and 'P5' are located in the unformed billet. The locations of the five points are shown in Fig. 8.

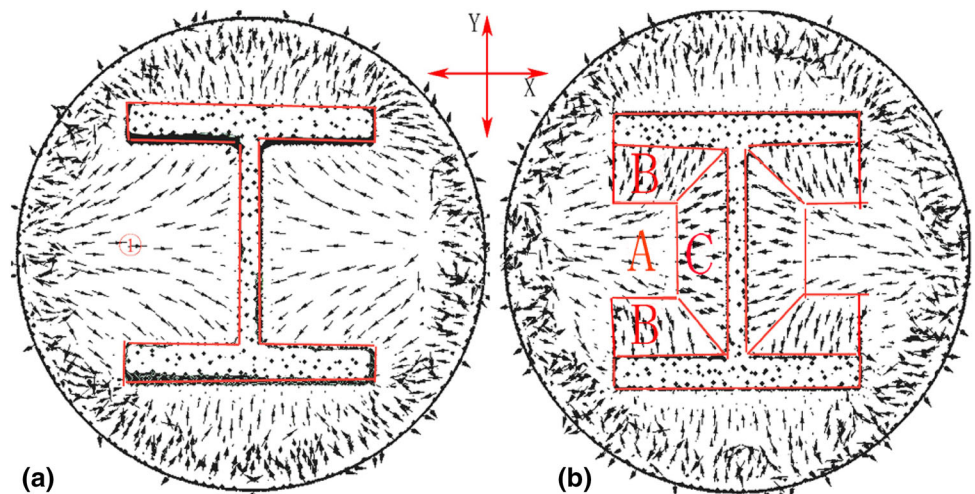
Figure 9a, b shows the strain change trend; the maximum strain of 'P4' and 'P5' is about 4.5, while that of 'P1', 'P2', and 'P3' is about 1.5. Figure 9c, d shows the strain rate change trend; the maximum strain rate of the flat-die is  $5 \text{ s}^{-1}$  larger than that of the cone-die. Figure 9e, f shows the stress change trends of the flat-die and cone-die. The metal at 'P1', 'P2' and 'P3' flows almost synchronously, and deformation is completed in 0.5 s. 'P4' and 'P5' are at a distance from the die holes and lag slightly, and deformation is completed in 1.0 s. At the temperature of 1493 K, the maximum stresses of the flat-die and cone-die are 95 MPa and 90 MPa, respectively. Figure 9g, h shows the velocity change trend; the metal flow of the cone-die is more stable than that of the flat-die.

#### 3.1.2 Extrusion force changes with temperature and speed

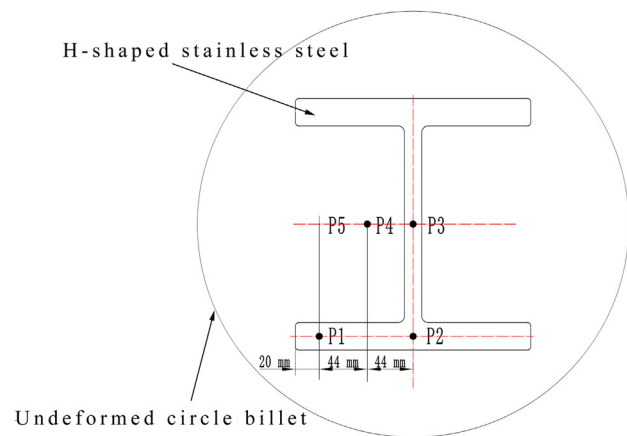
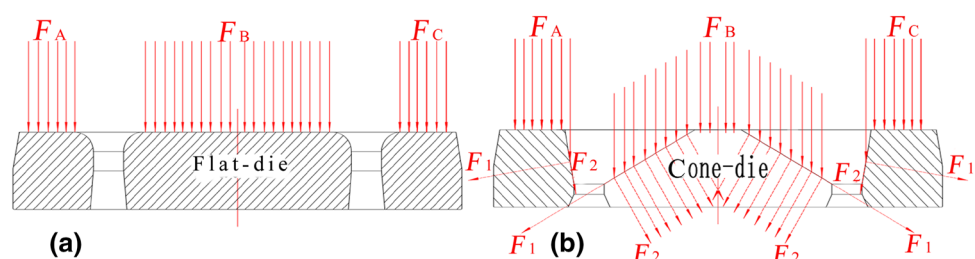
Figure 10a shows extrusion force curves of the cone-die at different speeds at a temperature of 1473 K. The extrusion force remains unchanged as speed increases, the breakthrough extrusion force values are 36.75 MN, 36.31 MN, 38.72 MN, 37.57 MN, 36.14 MN, and 35.69 MN at speeds of 150 mm/s, 200 mm/s, 250 mm/s, 300 mm/s, 350 mm/s, and 400 mm/s, respectively. The extrusion force values are all lower than 45 MN, and the extrusion time obviously reduces as the speed increases. When the speed exceeds 250 mm/s, the breakthrough extrusion force begins to decrease, because one part of the kinetic energy is converted into heat. Thus, deformation resistance decreases. This phenomenon can result in coarse grains or even defects, so the extrusion speed of 304L H-shaped stainless steel should be maintained below 250 mm/s.

Figure 10b shows extrusion force curves of the cone-die at different temperatures at a speed of 250 mm/s. The extrusion force decreases as temperature increases. The breakthrough extrusion force values are 47.44 MN, 45.09 MN, 41.54 MN, 39.05 MN, and 36.31 MN at temperatures of 1453 K, 1463 K, 1473 K, 1483 K, and 1493 K, respectively. To maintain the breakthrough extrusion force under 45 MN, the temperature should be higher than 1473 K.

**Fig. 6** Metal flow characteristics of the **a** flat-die and **b** cone-die



**Fig. 7** Transitive characteristic of the force: **a** flat-die and **b** cone-die



**Fig. 8** Five trace points and locations

### 3.2 Extrusion production

#### 3.2.1 Glass pad

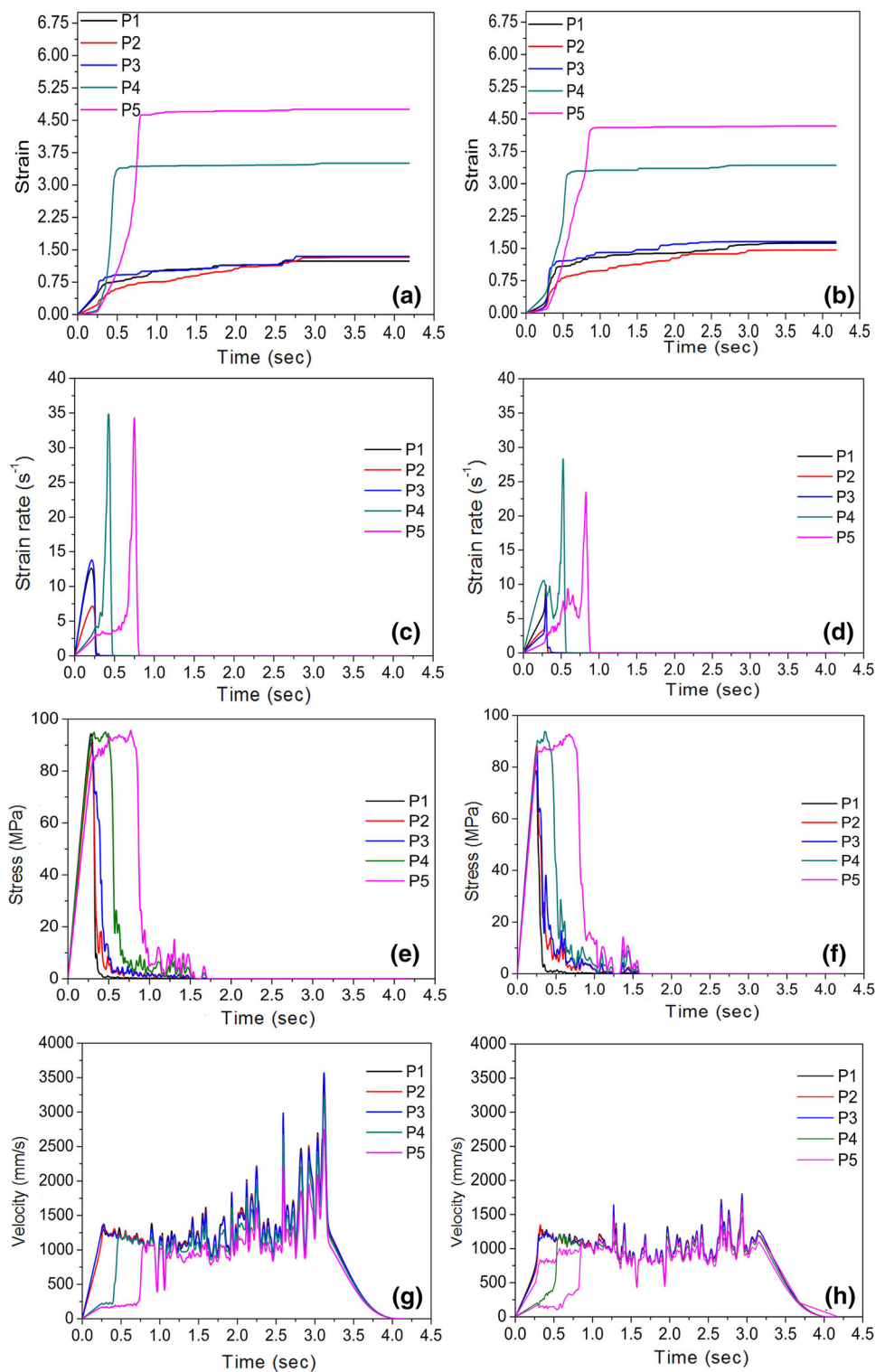
Figure 11a, b shows the tool and glass pad. The material of tool is plastic. The material of the glass pad is a mixture of glass powder, sodium silicate and water, which is heated to 473 K and retained for 2 h in a resistance furnace. When the extrusion deformation of 304L H-shaped stainless steel begins, the glass pad is heated rapidly, the glass softens

into a viscous state with the extrusion force and heat, and glass adheres to the surface of the metal to form a glass film. The glass film is driven out of the extrusion die hole with the metal and provides lubrication. A thin, black layer of glass film adheres to the surface of the H-shaped stainless steel.

#### 3.2.2 Heating curves

Figure 12a shows the heating curve of the circular furnace, which is divided into five zones. 'A1' is the pre-heating zone, and the target temperature is 1023 K. 'A2', 'A3', and 'A4' are the heating zones. The time in each zone is 0.5 h, and the target temperatures are 1073 K, 1133 K, and 1223 K, respectively. 'A5' is the soaking zone; the target temperature is 1223 K and the time is 1 h. Figure 12b shows the heating curve of the induction furnace, which is divided into four zones. 'B1' is the heating zone; the target temperature is 1493 K and the heating power is 500 kW. 'B2' and 'B3' are the heating preservation zones; the powers are 250 kW and 180 kW, respectively, at the temperature of 1493 K. In order to make up for the temperature drop, 'B4' is added, which is the final heating zone. In this zone, the temperature rapidly rises to 1533 K with the power of 550 kW.

**Fig. 9** (Color online) **a** Strain of flat-die, **b** strain of cone-die, **c** strain rate of flat-die, **d** strain rate of cone-die, **e** stress of flat-die, **f** stress of cone-die, **g** velocity of flat-die, and **h** velocity of cone-die



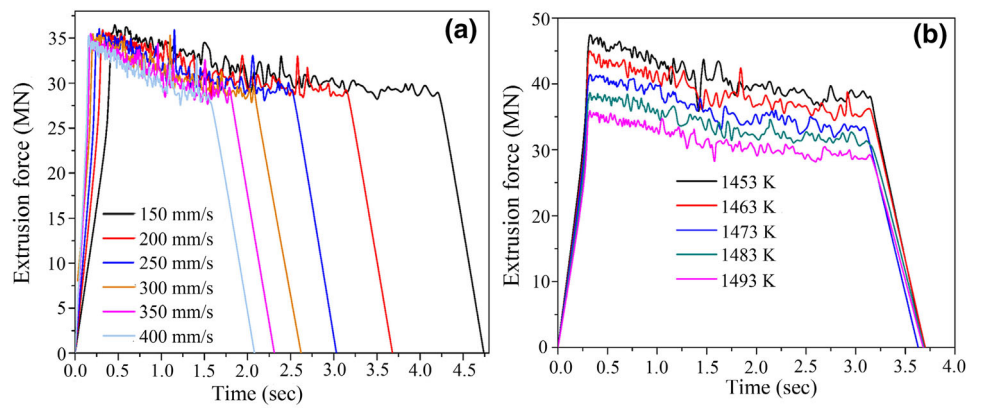
### 3.2.3 H-shaped stainless steel products and extrusion force curve

Based on the simulation results, the 304L H-shaped stainless steels are manufactured using a Germany SMS 60

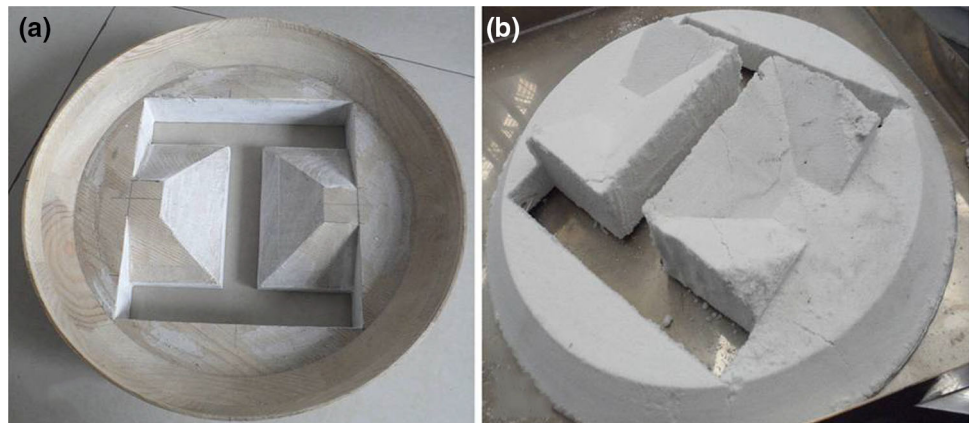
MN horizontal extruder, at a temperature of 1473 K and a speed of 250 mm/s.

Figure 13a shows three different production experiments. In failure case 'I', a flat-die (Fig. 3c) is adopted, the inner shape of the cushion is a circular hole, and the flat-die

**Fig. 10** (Color online) **a** Extrusion force changes with temperature and **b** extrusion force changes with temperature speed



**Fig. 11** **a** Tool and **b** glass pad



**Fig. 12** (Color online) **a** Heating curve of circular furnace and **b** heating curve of induction furnace

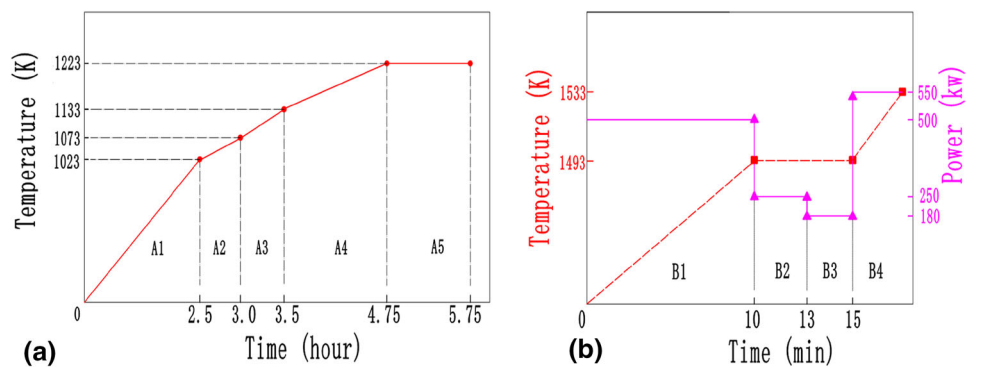
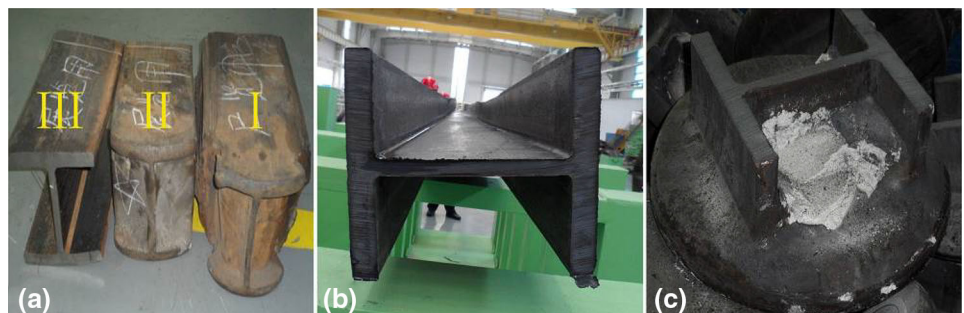


**Fig. 13** (Color online) **a** Production experiments, **b** 304L H-shaped stainless steel, and **c** surplus metal



and cushion all cracked. In failure case ‘II’, a flat-die is adopted, the inner shape of the cushion is H-shaped (Fig. 3b), but the inner shape of the glass pad is a circular hole. In successful case ‘III’, the cone-die (Fig. 14a) is adopted, and an H-shaped hole is designed in the cushion and glass pad, as shown in Figs. 3b and 11b. Figure 13b, c shows the successful 304L H-shaped stainless steel and surplus metal, respectively.

The 304L stainless steel circular billet is successfully deformed to H-shaped stainless steel at a temperature of 1473 K and a speed of 250 mm/s. Figure 14a shows the cone-die after extrusion. Figure 14b shows the extrusion force curve, which is divided into three stages. ‘C1’ is the breakthrough phase, with a peak value of about 47 MN. ‘C2’ is the stable phase, with a mean value of 40 MN, which is close to the simulated result. ‘C3’ is the unloading phase, with a peak value of 42 MN. The extrusion force increases slightly when extrusion stops.

Figure 15a shows the 304L H-shaped stainless steel after the pickling process. The pickling solution is a mixture of nitric acid (20%), hydrofluoric acid (10%), and water (70%). Figure 15b shows the dye penetration test after polishing according to the standard of RCC-M MC4000. Figure 15c shows the final products after fixed length. Figure 15d shows the welding assembly process of the support frame. These 304L H-shaped stainless steels were successfully used as the support frame of the PRHR HX in the Haiyang nuclear power plant.

### 3.2.4 Mechanical properties and microstructures

Figure 16a shows the sampling location of 304L H-shaped stainless steel according to GB/T 2975 (corresponding to ISO 377: 1997). Samples 1<sup>#</sup> and 2<sup>#</sup> were cut from two different 304L H-shaped stainless steels, which were selected according to the Heat No. The Heat Nos. of Sample 1<sup>#</sup> and Sample 2<sup>#</sup> are B3102498 and B3604718, respectively. Figure 16b, c shows equiaxed austenite microstructures of 304L H-shaped stainless steel. The grain

size is tested according to the ASTM E112-2013 standard. Refining grain size is one method to improve the strength of austenite stainless steels. Dynamic crystallization, metadynamic crystallization, and grain growth occurred successively during the extrusion process. The 304L H-shaped stainless steel is rapidly deformed by the extrusion process. The extrusion time is usually no more than 10 s at the high temperature, after which the hot-state 304L H-shaped stainless steel is annealed quickly in the cooling water. In order to guarantee the strength of the H-shaped stainless steel listed in Table 2, the grain size grade should not be smaller than four. Ravi Kumar [14] studied the effect of grain microstructure on the tensile properties and stress–strain curve of 304L. Mirzadeh [15] studied the hot deformation behavior of AISI 304L austenitic stainless steel. After the solution annealing process, the fine grain size can obviously improve the mechanical properties. Table 2 shows the concrete values of solution annealed mechanical properties and grain size grade. All mechanical properties and microstructure meet the requirements of application performance.

## 4 Conclusion

Analysis of the characteristics of metal flow, force transitive on the die, and production experiments show that the cone-die is favorable for metal flow and for decreasing the extrusion force. A speed less than 250 mm/s can decrease the risk of product defects, and a temperature greater than 1473 K can guarantee that the extrusion force remains under 45 MN. A  $\Phi$ 388-mm circular forging billet,  $\Phi$ 400-mm extrusion container, circular furnace, and an induction furnace can satisfy the dimensions of the 304L H-shaped stainless steel, cushion, and glass pad with an H-shaped hole and ensure that the metal flows out smoothly. After pickling and polishing, the surfaces of the 304L H-shaped stainless steel products pass the dye penetration

**Fig. 14** a Cone-die and b extrusion force curve

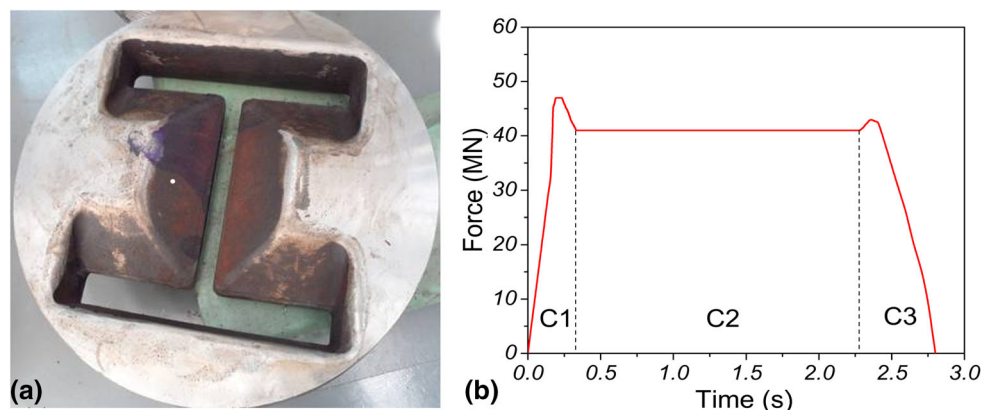


**Fig. 15** (Color online) **a** Surface after acid pickling, **b** dye penetration test, **c** final products, and **d** manufacture of the support frame

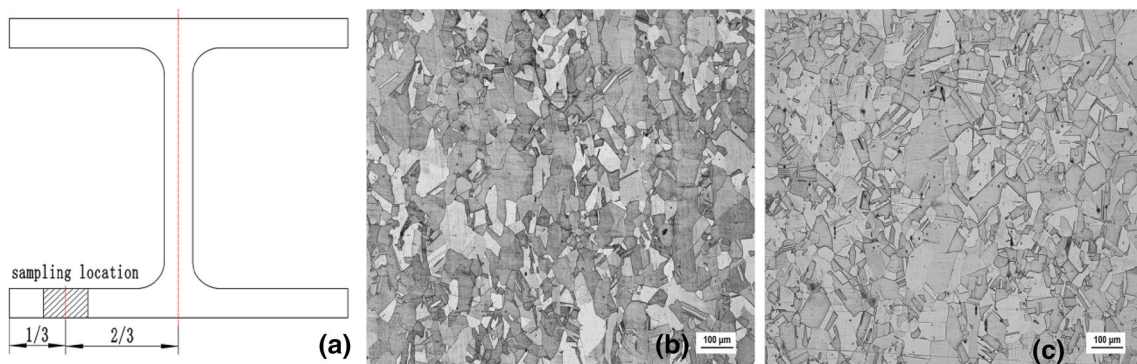
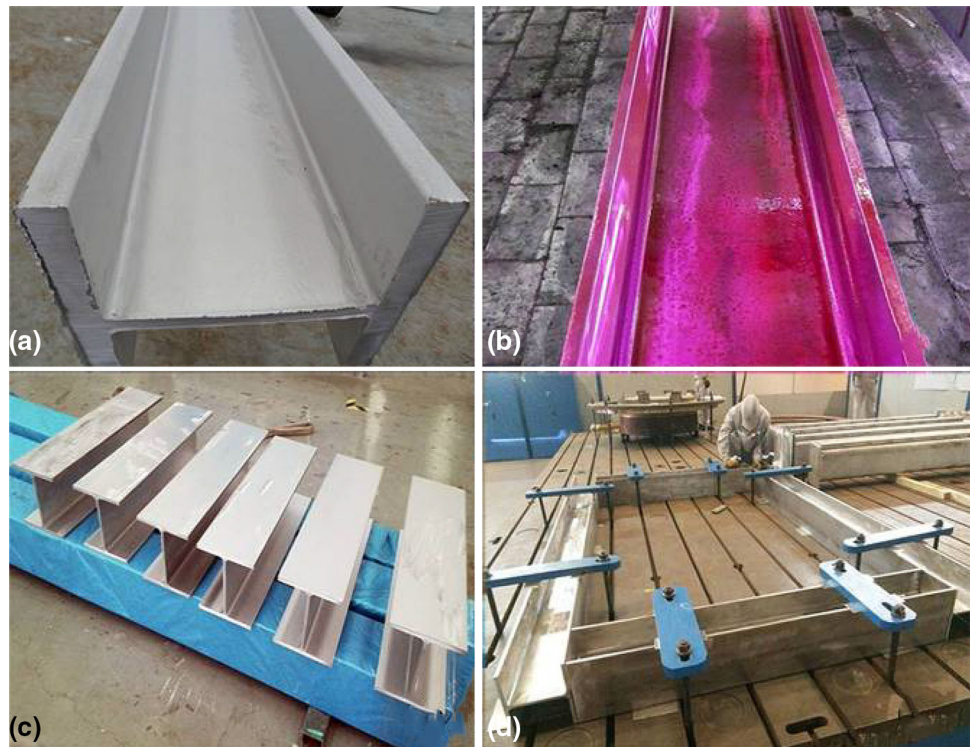


**Fig. 16** **a** Sample location, **b** microstructure of Sample 1<sup>#</sup>, and **c** microstructure of Sample 2<sup>#</sup>

**Table 2** Mechanical properties of 304L H-shaped stainless steel

Mechanical properties	Yield strength	Tensile strength	Brinell hardness	Total elongation	Reduction of area	Grain size number
Requirement	≥ 205 MPa	≥ 515 MPa	≤ 92	≥ 30%	≥ 40%	≥ 4
Sample 1 <sup>#</sup>	285/287	625/620	84.5/87/86	60/63	76/74	6/5
Sample 2 <sup>#</sup>	289/295	645/635	85.5/87/87	62/62	72/75	6/6

test. All mechanical properties and microstructures also meet the requirements of application performance.

**Acknowledgements** The research presented in this paper is partially funded by the Stainless steel tube branch company, Taiyuan Iron & Steel (Group) CO. LTD. The 304L stainless billet and extrusion productive experiment condition are provided by them. The authors

also thank laboratory engineer Xiao-Wen Zhang for his assistance in conducting the tensile tests and metallographic test at the Technology Center Laboratory, Taiyuan Iron & Steel (Group) CO. LTD.

## References

1. J.S. Wan, S.F. Wu, A. Nuerlan et al., Dynamic modeling of AP1000 steam generator for control system design and simulation. *Ann. Nucl. Energy* **109**, 648–657 (2017). <https://doi.org/10.1016/j.anucene.2017.05.016>
2. S.J. Rose, J.N. Wilson, N. Capellan et al., Minimization of actinide waste by multi-recycling of thoriated fuels in the EPR reactor. *Ann. Nucl. Energy* **38**, 2619–2624 (2011). <https://doi.org/10.1016/j.anucene.2011.06.029>
3. D.C. Sun, Y. Li, Z. Xi et al., Experimental evaluation of safety performance of emergency passive residual heat removal system in HPR1000. *Nucl. Eng. Des.* **318**, 54–60 (2017). <https://doi.org/10.1016/j.nucengdes.2017.04.003>
4. D.G. Lu, Y.H. Zhang, Z.Y. Wang et al., Numerical and experimental investigation on the baffle design in secondary side of the PRHR HX in AP1000. *Ann. Nucl. Energy* **94**, 359–368 (2016). <https://doi.org/10.1016/j.anucene.2016.04.003>
5. W. Karlsen, G. Diego, B. Devrient, Localized deformation as a key precursor to initiation of intergranular stress corrosion cracking of austenitic stainless steels employed in nuclear power plants. *J. Nucl. Mater.* **406**, 138–151 (2010). <https://doi.org/10.1016/j.jnucmat.2010.01.029>
6. V. Shankar Rao, J. Lim, I. Soon Hwang, Analysis of 316L stainless steel pipe of lead–bismuth eutectic cooled thermo-hydraulic loop. *Ann. Nucl. Energy* **48**, 40–44 (2012). <https://doi.org/10.1016/j.anucene.2012.05.009>
7. S.L. Wang, B. Yang, M.X. Zhang et al., Numerical simulation and experimental verification of microstructure evolution in large forged pipe used for AP1000 nuclear power plants. *Ann. Nucl. Energy* **87**, 176–185 (2016). <https://doi.org/10.1016/j.anucene.2015.07.042>
8. Y.H. Zhang, D.G. Lu, Z.Y. Wang et al., Experimental investigation on pool-boiling of C-shape heat exchanger bundle used in PRHR HX. *Appl. Therm. Eng.* **114**, 186–195 (2017). <https://doi.org/10.1016/j.applthermaleng.2016.11.185>
9. Z.F. Cai, J.M. Zhao, P. Zhao et al., Manufacture of W-shaped stainless steel and square shaped stainless steel to be used as the support for AP1000 passive residual heat removal heat exchanger. *China Nucl. Power* **7**, 240–244 (2014). **(in Chinese)**
10. L. Wang, X.J. Xu, The welding for AP1000 passive residual heat removal heat exchanger. *Boiler Manuf.* **6**, 39–42 (2015). **(in Chinese)**
11. L. Wang, Analysis of the key manufacturing process for AP1000 china-made passive residual heat removal heat exchanger. *Press. Vessel Technol.* **29**, 39–42 (2012). **(in Chinese)**
12. S. Hansson, T. Jansson, Sensitivity analysis of a finite element model for the simulation of stainless steel tube extrusion. *J. Mater. Process. Technol.* **210**, 1386–1396 (2010). <https://doi.org/10.1016/j.jmatprotec.2010.03.028>
13. C.Y. Liu, R.J. Zhang, Y.N. Yan et al., Lubrication behavior of the glass lubricated hot extrusion process. *J. Mech. Eng.* **47**, 127–134 (2011). <https://doi.org/10.3901/JME.2011.20.127>
14. B. Ravi Kumar, S. Sharma, B.P. Kashyap et al., Ultrafine grained microstructure tailoring in austenitic stainless steel for enhanced plasticity. *Mater. Des.* **68**, 63–71 (2015). <https://doi.org/10.1016/j.matdes.2014.12.014>
15. H. Mirzadeh, M.H. Parsa, D. Ohadi, Hot deformation behavior of austenitic stainless steel for a wide range of initial grain size. *Mater. Sci. Eng. A Struct.* **569**, 54–60 (2013). <https://doi.org/10.1016/j.msea.2013.01.050>